Biomaterials 80 (2016) 20–32

Contents lists available at ScienceDirect

Biomaterials

journal homepage: www.elsevier.com/locate/biomaterials

Combined sonodynamic and antimetabolite therapy for the improved treatment of pancreatic cancer using oxygen loaded microbubbles as a delivery vehicle

Conor McEwan [a], Sukanta Kamila [a], Joshua Owen [b], Heather Nesbitt [a], Bridgeen Callan [a], Mark Borden [c], Nikolitsa Nomikou [d], Rifat A. Hamoudi [d], Mark A. Taylor [e], Eleanor Stride [b, ***], Anthony P. McHale [a, **], John F. Callan [a, *]

[a] Biomedical Sciences Research Institute, University of Ulster, Coleraine, Northern Ireland, BT52 1SA, UK
[b] Institute of Biomedical Engineering, University of Oxford, OX3 7DQ, UK
[c] Department of Mechanical Engineering, University of Colorado, 1111 Engineering Drive, Boulder, CO 80309, USA
[d] Division of Surgery & Interventional Science, Faculty of Medical Sciences, University College London, UK
[e] Department of HPB Surgery, Mater Hospital, Belfast, Northern Ireland, BT14 6AB, UK

ARTICLE INFO

Article history:
Received 13 October 2015
Received in revised form
23 November 2015
Accepted 24 November 2015
Available online 26 November 2015

Keywords:
Hypoxia
Microbubbles
SDT
Rose Bengal
5-Flurouracil
Cancer
Pancreatic

ABSTRACT

In this manuscript we describe the preparation of an oxygen-loaded microbubble (O_2MB) platform for the targeted treatment of pancreatic cancer using both sonodynamic therapy (SDT) and antimetabolite therapy. O_2MB were prepared with either the sensitiser Rose Bengal (O_2MB-RB) or the antimetabolite 5-fluorouracil (O_2MB-5FU) attached to the microbubble (MB) surface. The MB were characterised with respect to size, physical stability and oxygen retention. A statistically significant reduction in cell viability was observed when three different pancreatic cancer cell lines (BxPc-3, MIA PaCa-2 and PANC-1), cultured in an anaerobic cabinet, were treated with both SDT and antimetabolite therapy compared to either therapy alone. In addition, a statistically significant reduction in tumour growth was also observed when ectopic human xenograft BxPC-3 tumours in SCID mice were treated with the combined therapy compared to treatment with either therapy alone. These results illustrate not only the potential of combined SDT/antimetabolite therapy as a stand alone treatment option in pancreatic cancer, but also the capability of O_2-loaded MBs to deliver O_2 to the tumour microenvironment in order to enhance the efficacy of therapies that depend on O_2 to mediate their therapeutic effect. Furthermore, the use of MBs to facilitate delivery of O_2 as well as the sensitiser/antimetabolite, combined with the possibility to activate the sensitiser using externally applied ultrasound, provides a more targeted approach with improved efficacy and reduced side effects when compared with conventional systemic administration of antimetabolite drugs alone.

1. Introduction

Pancreatic cancer remains one of the most lethal types of cancer known with less than 20% of those diagnosed being eligible for curative surgical treatment [1]. It accounts for approximately 2% of all cancers with a five year survival of 15–21%, only in those who have a surgical resection followed by systemic chemotherapy [2]. Conventional treatment often involves major surgery, chemotherapy, radiotherapy or combinations of all of these [3]. All three interventions may result in various complications including sepsis. Therefore, the development of more targeted and less invasive therapeutic approaches with improved efficacy to treat such patients is highly sought after.

Recently, we have demonstrated the effectiveness of sonodynamic therapy (SDT) for the treatment of pancreatic cancer in a preclinical model [4]. SDT has emerged as an alternative to the more established photodynamic therapy (PDT) as a potential anti-cancer treatment [5]. Both approaches involve the localised activation of

* Corresponding author.
** Corresponding author.
*** Corresponding author.
E-mail addresses: eleanor.stride@eng.ox.ac.uk (E. Stride), ap.mchale@ulster.ac.uk (A.P. McHale), j.callan@ulster.ac.uk (J.F. Callan).

http://dx.doi.org/10.1016/j.biomaterials.2015.11.033
0142-9612/

an otherwise non-toxic sensitiser by a stimulus (light in the case of PDT and low intensity ultrasound in the case of SDT) resulting in the generation of reactive oxygen species (ROS), in particular the potent intracellular cytotoxic singlet oxygen [6]. However, the poor penetration of light through human tissue has limited PDT to the treatment of superficial lesions and restricts its ability to treat more deeply-seated and anatomically less accessible lesions [7]. SDT offers some significant advantages over PDT: ultrasound is widely accepted as a cost effective and safe clinical imaging modality and, unlike light, can be tightly focused with penetration in soft tissue up to several tens of centimetres depending on the frequency used [8]. Our previous results have also demonstrated that an injection of ultrasound-responsive microbubbles (MB), filled with gaseous oxygen and bearing a Rose Bengal sensitiser, provided a statistically significant SDT-mediated reduction in tumour growth using mice bearing human xenograft BxPC-3 tumours when compared to tumours treated with a similar MB conjugate comprising SF_6 as the core gas [4]. The rationale for the incorporation of oxygen in the core of the MB was to enhance the amount of ROS generated in the tumour microenvironment during the sonodynamic event, as oxygen is a substrate for ROS production in SDT [9]. Pancreatic tumours, in particular, are known to be highly hypoxic and this further negatively impacts the efficacy of approaches such as PDT/SDT as well as stereotactic radiotherapy that depend on oxygen for the generation of cytotoxic ROS [10].

It has also been demonstrated that combining the benchmark pancreatic cancer antimetabolite therapeutics 5-fluorouracil (5-FU) and gemcitabine with complimentary chemotherapies such as irinotecan and oxaliplatin can improve the mean survival rate for pancreatic cancer sufferers [11]. However, this combination, known as FOLFIRINOX, results in significant side effects and is only indicated for patients who are otherwise fit and healthy. We hypothesise that as antimetabolite therapy and SDT exert their cytotoxic effects via different mechanisms (the former through thymidylate synthase inhibition [12] and the latter through oxidation of cellular substrates [13]) their combination in a single therapeutic regime may provide significant patient benefit. Furthermore, by utilising an oxygen loaded MB platform in combination with externally applied ultrasound to deliver not only oxygen, but also the antimetabolite and sensitiser to the tumour microenvironment, a highly targeted therapy can be realised, particularly as a result of increasing the therapeutic indices of the sensitiser and the antimetabolite chemotherapeutic drug. This would be expected to reduce chemotherapy-associated side effects and would, in turn, provide significant patient benefit.

Here, we describe the preparation of oxygen-loaded lipid-stabilised MBs (O_2MB) with either Rose Bengal (O_2MB-RB) or 5-FU (O_2MB-5FU) attached to their surface. We characterise the resulting conjugates in terms of MB stability and ultrasound-mediated oxygen release and demonstrate ultrasound-mediated cytotoxicity of combined antimetabolite/SDT treatment in a panel of pancreatic cancer cell lines *in vitro*. We demonstrate therapeutic efficacy of the combined approach using a preclinical ectopic human xenograft pancreatic tumour model in mice and compare this with conventional therapeutic approaches exploiting 5-FU or gemcitabine treatment alone. Furthermore we provide preliminary evidence to suggest that SDT has a significant impact on signal transduction processes that mediate the immune response and cell proliferation.

2. Materials and methods

2.1. Reagents and equipment

Rose bengal sodium salt, 2-bromoethylamine, NHS-biotin, MTT, avidin, FITC avidin, chloroacetic acid, 4-dimethylaminopyridine (DMAP), hydroxybenzotriazole (HOBt), N,N′-dicyclohexylcarb-odiimide (DCC), anhydrous dimethylformamide (DMF) and ethanol were purchased from Sigma Aldrich (UK) at the highest grade possible. Biotin, 5-Flurouracil, di(N-succinimidyl)carbonate and 2-aminoethanol were purchased from Tokyo Chemical Industry UK Ltd. 1,2-dibehenoyl-sn-glycero-3-phosphocholine (DSPC), dibehenoylphosphatidylcholine (DBPC), 1,2-distearoyl-sn-glycero-3-phosphoethanolamine-N-[amino(polyethylene glycol)-2000 (DSPE-PEG (2000)) and DSPE-PEG(2000)-biotin were purchased from Avanti Polar Lipids (Alabaster, Alabama, USA). Oxygen gas was purchased from BOC Industrial Gases UK, while perfluorobutane (PFB) gas was purchased from Apollo Scientific Ltd. Phosphate Buffered Saline (PBS) was purchased from Gibco, Life Technologies, UK. NMR spectra were recorded on a Varian 500 MHz spectrometer. ESI-MS characterisation was achieved using a LCQTM quadrupole ion-trap mass spectrometer (Finnigan MAT, San Jose, California, USA) utilising electrospray ionisation (ESI). Optical microscope images were taken with an optical microscope (Leica DM500 optical microscope). Dissolved oxygen was measured using a Thermo Scientific Orion Star A216 bench top dissolved oxygen metre. Error was expressed as ± SEM (standard error of the mean) while statistical comparisons were made using an un-paired student's t-test.

2.2. Preparation of O_2 loaded microbubbles

DSPC MBs were prepared as described in our previous communication [4]. For the preparation of DBPC MBs, DBPC (4.0 mg, 4.43 μmol), DSPE-PEG (2000) (1.35 mg, 0.481 μmol) and DSPE-PEG (2000)-biotin (1.45 mg, 0.481 μmol) in a molar ratio of 82:9:9 were dissolved in chloroform and placed in a glass vial. The solution was heated at 40 °C until all the chloroform had evaporated. PBS (pH 7.4 ± 0.1) (5 ml) was added to the dried lipid film and the contents heated above the lipid phase transition temperature (>70 °C) under constant magnetic stirring for 30 min. The suspension was then sonicated with a Microson ultrasonic cell disruptor for 1.5 min (100 Watts, 22.5 kHz at power setting 4), the headspace filled with perfluorobutane (PFB) gas and the gas/liquid interface sonicated (power 19) for 20 s producing PFBMBs. The MB suspension was cooled in an ice bath for approximately 10 min. An aqueous solution of avidin (50 μL, 10 mg/mL) was then added to the cooled MB suspension and stirred for a further 10 min. The suspension was then centrifuged (300 RPM, 10 min) and the resulting MB "cake" concentrated into 1 mL of PBS (pH 7.4 ± 0.1). This was divided into two freeze drying vials. For the PFBMBs the vials were then crimped (sealed with a metal cap). To create oxygen filled MBs the headspace of the vial and the MB suspension was sparged under a positive pressure of oxygen gas for 2 min and the vial was then crimped. Following preparation as described above, MB samples were imaged under conventional optical microscopy to determine their size distribution and concentration. 10 μL samples were removed from each suspension and diluted in 90 μL of PBS (pH 7.4 ± 0.1) followed by examination on a haemocytometer (Bright-Line, Hausser Scientific, Horsham, PA, USA). Images were obtained with a 40× objective lens with a Leica DM500 optical microscope. The MB size distribution and concentration were then obtained using purpose written image analysis software in Matlab (2010B, The MathWorks, Natick, MA, USA).

2.3. Preparation of biotinylated Rose Bengal and biotinylated 5-FU

The preparation of biotin functionalised Rose Bengal (**6**) has been described by us in an earlier communication [4]. Biotin functionalised 5-FU (**5**) was synthesized according to Scheme 1a following the procedures outlined below.

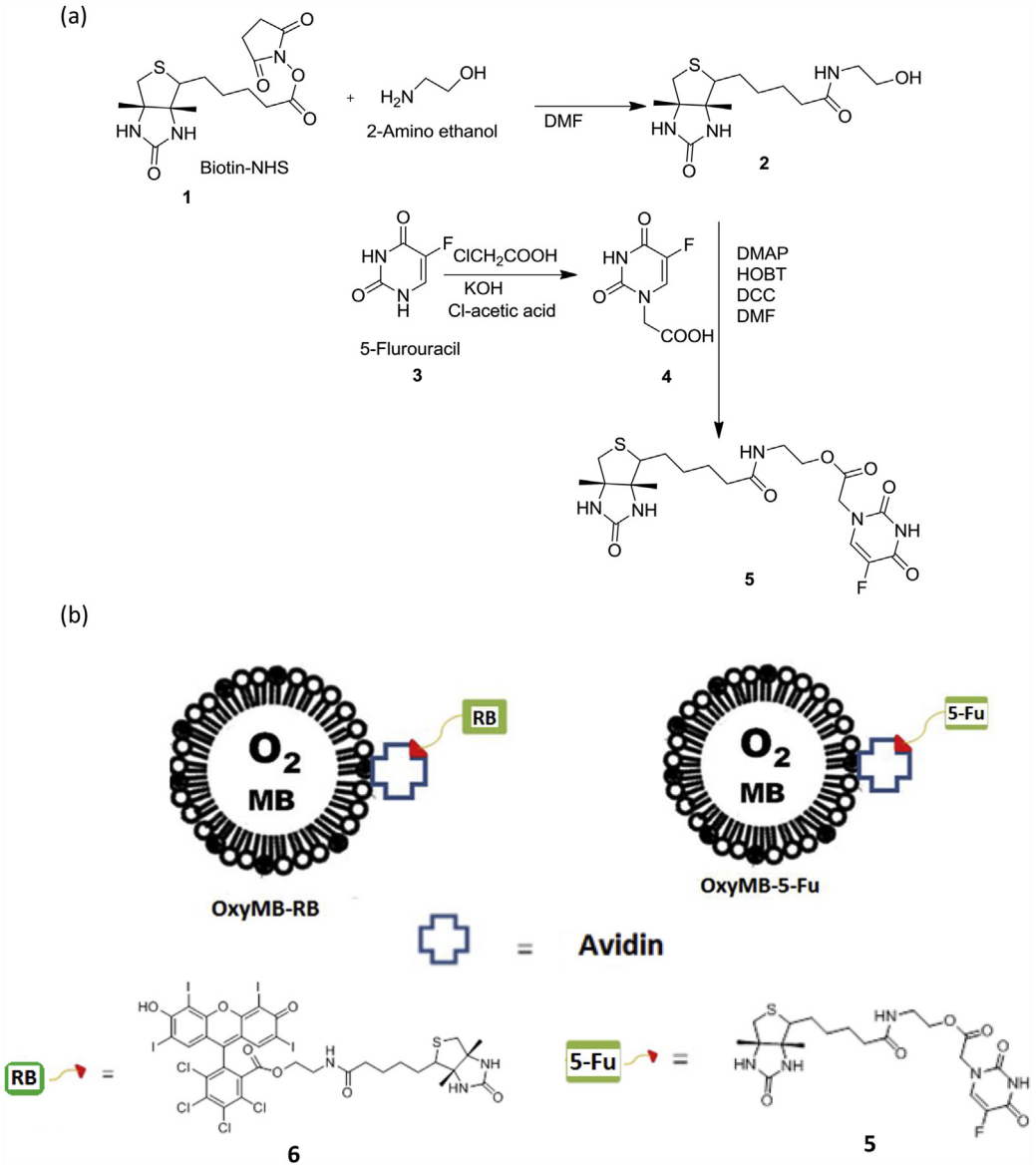

Scheme 1. (a) Synthetic scheme for the preparation of biotin-5-FU (**5**). (b) Schematic representation for the structure of the O_2MB-RB and O_2MB-5FU conjugates.

2.3.1. Preparation N-(2-hydroxyethyl)-5-(2-oxohexahydro-1H-thieno[3,4-d]imidazol-4-yl)pentanamide (2)

To an ice-cooled solution of biotin-*N*-hydroxysuccinimide ester (**1**) (prepared by the reaction between biotin and Di(*N*-succinimidyl)carbonate) [14], (3.75 g, 11 mmol) in anhydrous DMF (40 mL), was added 2-aminoethanol (1.0 ml, 16.4 mmol) and the mixture stirred at 25 °C for 30 min. The reaction was monitored by thin layer chromatography (TLC) (Merck Silica 60, HF 254, 20:80 methanol-dichloromethane v/v). The biotin-*N*-hydroxysuccinimide ester (R_f = 0.76) was consumed within 15 min with the concomitant formation of the alcohol product (R_f = 0.47). The reaction mixture was concentrated under reduced pressure and the residue co-evaporated with DMF to remove excess amounts of 2-aminoethanol. The white residue was recrystallized from water to yield **2** as a light yellow solid (1.7 g, 38%). An analytical sample was obtained from a second recrystallization, m.p. 192–195 °C, ^{1}H NMR (500 MHz, D_2O) 4.49–4.47 (m, 1H, –CH), 4.31–4.30 (m, 1H, –CH), 3.53–3.51 (m, 2H, CH_2), 3.23-3.18 (m, 3H, CH and CH_2), 2.85–2.64 (m, 2H, CH_2), 2.15 (t, 2H, $-CH_2$), 1.62–1.46 (m, 4H, CH_2 X 2), 1.32–1.26 (m, 2H, CH_2). ^{13}C NMR (125 MHz, D_2O) 177.09 (C=O), 61.98 (CH_2), 60.19 (CH), 59.91 (CH), 55.24 (CH), 41.29 (CH_2), 39.61 (CH_2), 35.42 (CH_2), 27.77 (CH_2), 27.56 (CH_2), 25.02 (CH_2). ESMS ($M+H^+$): found 288.70, calculated for $C_{12}H_{21}N_3O_3S$ = 287.13.

2.3.2. Preparation of 5-fluorouracil-1-carboxylic acid (4)

A mixture of 5-Fluorouracil (**3**) (5 g, 38.4 mmol), potassium hydroxide (9.07 g, 161.6 mmol) and chloroacetic acid (3.63 g, 38.4 mmol) in 100 mL of water was refluxed for 2 h at 70 °C. After cooling to room temperature, the pH of the solution was adjusted to 5.5 by the addition of concentrated hydrochloric acid. The reaction mixture was then kept in a refrigerator (5 °C) for 18 h and the resulting white crystals isolated by filtration and washed with cold water to produce **4** in 52.5% yield. mp > 200 °C, ^{1}H NMR (500 MHz, D_2O) 7.76 (d, 1H, J = 6 Hz, CH), 4.29 (s, 2H, CH_2). ^{13}C NMR (D_2O): 173.58 (C=O), 159.97 (C=O), 150.80 (C=O), 141.20 (C), 131.74 (CH), 51.48 (CH_2). ESMS ($M-H^+$): found 187.10, calculated for $C_6H_5O_4N_2F$ = 188.11.

2.3.3. Preparation of 2-(5-(2-oxohexahydro-1H-thieno[3,4-d] imidazol-4yl)pentanamido) ethyl 2-(5-fluoro-2,4-dioxo-3,4-dihydropyrimidin-1(2H)-yl)acetate (5)

N-(2-Hydroxyethyl)-5-(2-oxohexahydro-1*H*-thieno[3,4-*d*]imidazol-4-yl)pentanamide (**2**) (0.5 g, 1.7 mmol), 5-Fluorouracil-1-carboxylic acid (**4**) (0.4 g, 2.1 mmol), DMAP (0.023 g, 0.17 mmol) and HOBT (0.023 g, 0.17 mmol) were added to 20 mL of anhydrous DMF in a 100 mL 2-neck round bottom flask under a N_2 atmosphere. The mixture was heated at 40 °C and stirred until a homogeneous solution was obtained. DCC (0.4 g, 1.9 mmol) was then added to the reaction mixture and allowed to stir at room temperature for 12 h. The DMF was removed under reduced pressure, diethyl ether (50 mL) added and the contents stirred for 20 min. The resulting white semi-solid product was removed by filtration and after removing excess diethyl ether under reduced pressure, the crude product was purified by preparative HPLC (C-18 column) using acetonitrile/water (80:20 v/v) as mobile phase. The product **5** was obtained after lyophilisation of the desired fractions as a white semi-solid (0.24 g, 30% Yield). ^{1}H NMR (500 MHz, D_2O): 7.67 (d, 1H, J = 6.0 Hz, CH), 4.50–4.47 (m, 1H, CH), 4.31–4.29 (m, 1H, CH), 4.19 (s, 2H, CH_2), 3.54 (t, 2H, CH_2), 3.22–3.19 (m, 2H, CH_2), 2.89–2.86 (m, 1H, CH), 2.67–2.64 (m, 2H, CH_2), 2.17–2.14 (m, 2H, CH_2), 1.61–1.47 (m, 4H, CH_2 X 2), 1.47–1.28 (m, 2H, CH_2). ^{13}C NMR 125 MHz, D_2O): 177.12 (C═O),173.74 (C═O), 165.33 (C═O), 160.01 (C═O), 159.81 (C═O), 141.14 (C), 131.71 (CH), 62.00(CH_2), 60.22 (CH), 59.94 (CH), 55.26 (CH), 51.53 (CH_2), 41.31 (CH_2), 39.64 (CH_2), 35.45 (CH_2), 27.79 (CH_2), 27.58 (CH_2), 25.14 (CH_2). ESMS ($M-H^+$) found 456.20, calculated for $C_{18}H_{24}FN_5O_6S$ = 457.48.

2.4. Preparation of O_2MB-Rose Bengal and O_2MB-5FU conjugates

Saturated solutions of **5** (91.2 mM) and **6** (0.61 mM) were prepared in a 0.5% DMSO solution in PBS (pH 7.4 ± 0.1). A 0.3 mL aliquot of these stock solutions were then added separately to two 1 mL suspensions of avidin functionalised PFBMBs (1×10^9 MB/mL) and the contents vortex mixed for 15 min. The suspensions were then centrifuged (900 rpm) for 5 min and the MB conjugates isolated as a milky suspension floating on top of the solution. The solution was removed and replaced with a further 0.3 mL of stock solution containing either **5** or **6** and the mixing/centrifugation steps repeated. The MB suspensions were then washed with PBS (5 mL), centrifuged (900 rpm) for 5 min and the MBs transferred to a clean centrifuge tube. This washing procedure was repeated again and the isolated PFBMB-RB and PFBMB-5FU conjugates placed in glass vial. The PFBMB-RB and PFBMB-5FU conjugates were then sparged with oxygen gas for 2 min and the resulting O_2MB-RB and O_2MB-5FU conjugates were mixed together at a ratio of 1: 3.25 to produce a final suspension containing 6.8×10^7 MB/mL with 90.8 μM RB and 440 μM 5-FU.

2.5. Synthesis of 2-((E)-2-((E)-2-((4-aminophenyl)thio)-3-((E)-2-(1,1-dimethyl-3-(4-sulfobutyl)-1H-benzo[e]indol-2(3H)-ylidene) ethylidene)cyclohex-1-en-1-yl)vinyl)-1,1-dimethyl-3-(4-sulfobutyl)-1H-benzo[e]indol-3-ium (8)

Compound **7** was prepared following a literature procedure [15]. 4-Aminothiophenol (0.63 g, 5 mmol) was dissolved in anhydrous DMF (50 ml) under N_2 atmosphere. **7** (0.6 g, 0.7 mmol) was added to this solution and the mixture stirred for 18 h at room temperature. The reaction was monitored by TLC (Merck Silica 60, HF 254, using 25% MeOH/DCM as mobile phase).The DMF was removed under reduced pressure and the residue re-dissolved in DMF (5 mL) and precipitated with Et_2O (15 mL). The solid product was filtered, washed with Et_2O (30 mL) and purified by column chromatography (silicagel, 60–120 mesh) using MeOH-DCM (1:3) as an eluting agent. The product (230 mg, 4.8%) was isolated as reddish brown semi-solid. This compound was not stable and was used immediately in the next step. ^{1}H NMR (500 MHz, MeOH-d_4): 8.96–8.93 (m, 2H, Ar-CH), 8.81–8.78 (m, 2H, Ar-CH), 8.09–8.07 (m, 2H, Ar-CH), 7.90–7.89 (m, 6H, Ar-CH), 7.57–7.51 (m, 4H, Ar-CH), 7.38 (brs, 2H, NH_2), 7.38–7.28 (m, 2H, Ar-CH), 6.34–6.31 (m, 2H, CH X 2), 4.23 (brs, 4H, CH X 2, CH_2), 2.87–2.80 (m, 8H, CH_2 X 4), 1.98–1.91 (m, 10H, CH_2 X 5), 1.70 (s, 12H, CH_3 X 4). ^{13}C NMR (125 MHz, dmso-d_6): 173.4, 170.2, 150.1, 148.4, 143.7, 144.6, 142.7, 134.3, 133.9, 132.4, 128.0, 126.1126.2, 125.5, 125.7, 117.5, 115. 4, 104.7, 61.8, 59.3, 49.4, 48.9, 46.8, 30.2, 28.6, 26.8, 26.9, 25.2, 21.0. ESMS calculated for $C_{52}H_{58}N_3O_6S_3Na_2^+$ = 961.1, found 960.3.

2.6. Synthesis of 2-((E)-2-((E)-3-((E)-2-(1,1-dimethyl-3-(4-sulfobutyl)-1H-benzo[e]indol-2(3H)-ylidene)ethylidene)-2-((4-(5-(2-oxohexahydro-1H-thieno[3,4-d]imidazol-4-yl)penta namido) phenyl)thio)cyclohex-1-en-1-yl)vinyl)-1,1-dimethyl-3-(4-sulfobutyl)-1H-benzo [e]indol-3-ium (9)

Compound **8** (100 mg, 0.1 mmol) was added to a stirring solution of **1** (40.9 mg, 0.12 mmol) in anhydrous DMF (50 mL) to which a catalytic amount of triethylamine was added. The solution was stirred at room temperature for 5 h. The reaction mixture was added to ether (100 ml) and the contents stirred for 30 min. The precipitate was collected by filtration and purified by preparative TLC using MeOH: DCM (1:4) as eluting agent and the product isolated as a green powder. Yield = 21 mg, 18.4%. ^{1}H NMR (500 MHz, MeOH-d_4): 8.77 (d, J = 7.8 Hz, 2H, Ar-CH), 8.21 (d, J = 7.5 Hz, 2H, Ar-CH), 8.03–7.99 (m, 2H, Ar-CH), 7.73 (d, J = 7.5 Hz, 2H, Ar-CH), 7.60–7.57 (m, 2H, Ar-CH), 7.47–7.44 (m, 2H, Ar-CH), 7.20–7.17 (m, 2H, Ar-CH), 7.16 (d, J = 12 Hz, 1H, CH), 6.89–6.83 (m, 2H, Ar-CH), 6.58 (d, J = 12 Hz, 1H, CH), 6.42 (brs, 1H, NH), 6.36 (brs, 2H, NH X 2), 4.29–4.27 (m, 6H, CH X 2, NCH_2), 4.10 (brs, 2H, $-CH_2$), 3.14–3.06 (m, 3H, CH, CH_2), 2.80–2.74 (m, 4H, CH_2 X 2), 2.57–2.48 (m, 4H, CH_2 X 2), 2.19–2.16 (m, 2H, CH_2), 1.88–1.59 (m, 2H, CH_2), 1.76 (s, 12H, CH_3 X 4), 1.59–1.57 (m, 2H, CH_2), 1.48–1.28 (m, 12H, CH_2 X 6). ^{13}C NMR (125 MHz, dmso-d_6): 177.5, 174.3, 169.9, 166.2, 152.5, 150.2, 148.0, 145.3, 144.8, 140.7, 134.8, 132.6, 131.3, 130.0, 128.5, 126.3, 124.7, 120.1, 116.8, 114.8, 102.5, 64.0, 62.3, 60.1, 54.9, 50.1, 48.6, 48.1, 42.2, 36.7, 32.8, 30.2, 28.4, 28.3, 26.9, 26.0, 24.5, 22.8. ESMS calculated for $C_{62}H_{72}N_5O_8S_4^+$ = 1142.4 (protonated form, M^+), found 1143.4.

2.7. Preparation of O_2MB-IR820 conjugates

Biotin functionalised IR-820 (**9**) was attached to the surface of O_2MBs following the procedure as described in Section 2.4 for 5-FU and Rose Bengal. [**MB**] = 2.6×10^8; [**9**] = 280 μM.

2.8. Ultrasound mediated O_2 release from O_2MBs

A 0.5 mL suspension of O_2MBs (1×10^8) was added to degassed PBS (pH 7.4 ± 0.1) (4.5 mL). The dissolved oxygen level of this solution was measured over a 20 min period at 2 min intervals using a dissolved oxygen metre. Ultrasound was applied after 4.5 min for 1 min, using a frequency of 1 MHz, an ultrasound power density of 3.0 Wcm^{-2} and a duty cycle of 50% (pulse frequency = 100 Hz). Control experiments using PFBMBs were also performed following the same procedure.

2.9. In vitro cytotoxicity experiments

Human primary pancreatic adenocarcinoma cell lines MIA PaCa-2 and PANC-1 were maintained in Dulbecco's Modified Eagle's Medium while BxPC-3 cells were maintained in RPMI-1640

medium, all of which were supplemented with 10% (v/v) foetal bovine serum in a humidified 5% CO_2 atmosphere at 37 °C. These cell lines were plated into the wells of a 96-well plate at a concentration of 5×10^3 cells per well and incubated for 21 h at 37 °C in a humidified 5% CO_2 atmosphere before being transferred to a hypoxic chamber at 37 °C ($O_2/CO_2/N_2$, 0.1: 5: 94.9 v/v/v) for 3 h. The medium was then removed from each well and replaced with O_2MB-RB (50 μL, 5 μM RB) and O_2MB-5FU (50 μL, 100 μM 5FU) conjugates. Individual wells were then treated with ultrasound delivered using a Sonidel SP100 sonoporator (30 s, frequency = 1 MHz, ultrasound power density = 3.0 Wcm^{-2}, duty cycle = 50% with pulse repetition frequency = 100 Hz). Cells were kept in the hypoxic environment for a further 3 h before the treatment solution was removed, the cells washed with PBS and fresh media added (200 uL per well). Plates were then incubated in normoxic conditions (i.e. humidified 5% CO_2 atmosphere at 37 °C) for a further 21 h before cell viability was determined using a MTT assay [16]. A similar procedure was repeated for the vehicle only, gemcitabine, 5-FU, O_2MB-5FU + US, O_2MB-RB + US and the O_2MB-RB/O_2MB-5FU mix − US. In all experiments the amount of RB, 5-FU and gemcitabine used was 5 μM, 100 μM and 100 μM respectively. All groups were also repeated using PFBMB conjugates with the same amount of RB or 5-FU attached.

2.10. In vivo cytotoxicity experiments

All animals employed in this study were treated humanely and in accordance with licenced procedures under the UK Animals (Scientific Procedures) Act 1986. BxPc-3 cells were maintained in RPMI-1640 medium supplemented with 10% foetal calf serum as described above. Cells (1×10^6) were re-suspended in 100 μL of Matrigel® and implanted into the rear dorsum of female Balb/c SCID (C.B-17/IcrHan®Hsd-*Prkdcscid*) mice. Tumour formation occurred approximately 2 weeks after implantation and tumour measurements were taken every other day using callipers. Once the tumours had reached an average volume of 218 mm^3, calculated from the geometric mean diameter using the equation tumour volume = $4\pi R^3/3$, animals were randomly distributed into 10 groups (n = 4). Following induction of anaesthesia (intraperitoneal injection of Hypnorm/Hypnovel), a 100 μL mixture of PBS containing O_2MB-RB (MB = 1.6×10^7, [RB] = 90.8 μM) and O_2MB-5FU (MB = 5.2×10^7, [5FU] = 440 μM) was injected directly into each tumour. Intratumoural injection was chosen as the route of administration to preclude experimental variation resulting from pharmacokinetic behaviour of the platform. Where appropriate, tumours were then treated with ultrasound for 3.5 min at an ultrasound frequency of 1 MHz, an ultrasound power density of 3.5 Wcm^{-2} (I_{SATP}; spatial average temporal peak) and using a duty cycle of 30% at a pulse repetition frequency of 100 Hz. Additional treatment groups included (i) no drug (ii) O_2MB-RB conjugate alone ± ultrasound treatment (iii) O_2MB-5FU conjugate alone ± ultrasound treatment. Gemcitabine (440 μM) and 5-FU (440 μM) only treatments were also performed. After treatment, animals were allowed to recover from anaesthesia and tumour volume and body weight were recorded daily for nine days. The % increase in tumour volume was calculated employing the pre-treatment measurements for each group.

2.11. In vivo imaging of O_2MB-9 conjugates following IV administration to tumour bearing mice

Athymic nude mice were anaesthetised (intraperitoneal injection of Hypnorm/Hypnovel) and the O_2MB-**9** conjugate (100 uL) was administered via tail vein injection. In the treatment group, ultrasound (conditions as in 2.10 above) was applied to the tumours during and for 3 min after IV injection while no ultrasound was applied to the tumours in the control group (n = 3 in each group). Following administration (at t = 5 min and t = 10 min), animals were placed in the chamber of a Xenogen IVIS® Lumina imaging system on fluorescence mode using the ICG filter set (excitation: 705–780 nm; emission: 810–885 nm). Data were captured and analysed using the Living Image® software package version 2.60. Quantitative data were obtained by drawing a region of interest around the tumour and comparing the fluorescent signal (photons/second) at t = 5 and t = 10 min post O_2MB-**9** administration with the fluorescent signal obtained prior to administration.

2.12. HIF1α expression in the tumour post IV administration of O_2MB

Athymic nude mice were anaesthetised (intraperitoneal injection of Hypnorm/Hypnovel) and either PFBMBs or O_2MBs (100 uL) were administered via tail vein injection (n = 3 in each group). Ultrasound (conditions as in 2.10 above) was applied to the tumour during and for 3 min after IV injection and the tumours were excised 30 min later. For Western blotting analysis of HIF-1α protein expression, total protein was extracted using urea buffer. Primary murine antibodies employed in these studies were anti-HIF1α (Millipore, 1:500), and anti-GAPDH (Sigma, 1:1000). Protein samples were electrophoresed on a 4–12% TruPAGE® gel and transferred to nitrocellulose membranes. Blocking of non-specific binding was carried out in 5% (w/v) bovine serum albumin diluted in 1× tris buffered saline containing 0.05% (v/v) Tween 20. Membranes were then incubated in the appropriate secondary antibody, goat anti-mouse IgG-HRP (1:10,000 of the stock solution). Secondary antibodies were purchased from Santa Cruz Biotechnology, Heidelberg, Germany. Densitometry was carried out to quantify HIF1α protein expression using GAPDH as a housekeeping reference.

2.13. Immune response characterisation

To characterise the immune response in tissues subjected to therapy, Bcl3 and Bcl2 protein expression was examined using immunohistochemistry in tissue samples harvested at the end of the monitoring period. Immunohistochemical (IHC) evaluation for Bcl2 and Bcl3 proteins was performed on paraffin-embedded sections. The paraffin-embedded tissue samples were cut to a 4 μm thickness using a Leica RM2235 microtome (Leica Biosystems Ltd., Newcastle) and examined on a coated glass slide. IHC analysis for Bcl2 (clone: BCL-2/100/D5) and Bcl3 (clone: 1E8) were diluted 1:200 and 1:150 respectively. Both antibodies were mouse anti-human obtained from Leica Biosystems. Immunostaining was carried out using the automated Bond-Max system (Leica Biosystems Ltd., Newcastle) using on board heat-induced antigen retrieval with Bond Epitope Retrieval Solution 2 (EDTA based on pH 9.0) for 30 min. Endogenous peroxidase activity was blocked using 0.3% hydrogen peroxide for 5 min. The histological specimens were incubated with the primary antibody for 15 min at room temperature and the slides were incubated with rabbit anti-mouse for 8 min at room temperature. The slides were then incubated with goat anti-rabbit polymer reagent for 8 min at room temperature. The reactions were developed using a bond polymer refine detection kit and followed by colour development with 3,3′-diaminobenzidine tetrahydrochloride as a chromogen for 10 min. The immunohistochemistry intensity and proportion scores were carried out according to Allred et al. [17]. In order to confirm immunohistochemical studies Bcl3 expression was also examined at the transcriptional level., mRNA expression of Bcl3 was measured with gene specific qRT-PCR using the primers listed in Table S1. qRT-PCR

and analysis were performed following previously published protocols [18]. Briefly, RNA was extracted from microdissected slides using the RecoverAll Kit (Life Technologies, Paisley, UK). cDNA synthesis was carried out using the Superscript III First Strand cDNA synthesis kit (Life Technologies, Paisley, UK) using the reverse primer of each of the genes including the two housekeeping genes; 18S rRNA and β-actin. qRT-PCR was carried out using the SYBR Green kit on the CFX96 instrument (BioRad, UK). The qRT-PCR cycle was as follows: 95 °C for 3 min, 95 °C for 10 s, 60 °C for 45 s for 40 cycles. For analysis, the geometric mean of 18S rRNA and β-actin was taken as the single housekeeping value. Statistical comparison between the groups was carried out using two-way ANOVA with Bonferroni post-hoc analysis.

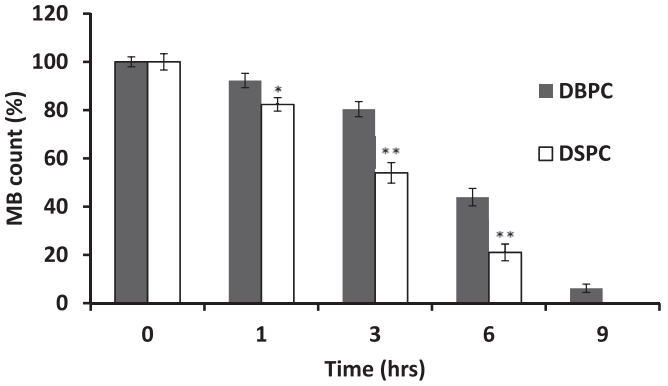

Fig. 2. Plot of % MB remaining after incubation of PBS dispersions of MBs prepared from either DBPC or DSPC at 37 °C. Error bars represent ± the standard error where n = 4. *p < 0.05 and **p < 0.01.

3. Results and discussion

Oxygen loaded lipid stabilised MBs (O_2MBs), surface functionalised with avidin, were prepared following a similar protocol to that outlined by us in an earlier communication [4]. However, to improve both the physical stability of the MBs and also their stability with respect to O_2 retention, we utilised the longer chain lipid dibehenoylphosphatidylcholine (DBPC) in place of distearoylphosphatidylcholine (DSPC) as this has been shown in previous work to reduce the diffusivity of the MB surface and hence improve stability [19]. These MBs had an average diameter of 1–2 μm with a concentration of approximately 1×10^9 MB/mL as determined by analysis of optical microscopy images (Fig. 1). To determine the effect that inclusion of DBPC had on MB stability, we incubated PBS dispersions of the MBs prepared with DBPC or DSPC at 37 °C and counted the number of viable MBs remaining at various time intervals. The results are shown in Fig. 2 and reveal a significant improvement in stability for MBs prepared from DBPC compared with those prepared using DSPC. Indeed, after 3 h incubation, 80% of DBPC MBs remained while the number of DSPC MBs reduced to 54%. These results are consistent with those from previous studies which showed that increasing the acyl chain length of the lipid reduced both the mechanical flexibility of the microbubbles and surface diffusivity [19].

If O_2MBs are to be successful as carrier for oxygen delivery *in vivo*, it is important that gas exchange between the core of the MB and blood is minimised until the MB is exposed to ultrasound at the target site. The half-life of commercial MBs ranges from 0.97 min in men to 1.23 min in women [20]. Therefore, it is important that O_2MBs can retain their oxygen for at least this time period in situations where an oxygen diffusion gradient may exist. In an attempt to simulate such a scenario, O_2MBs (0.5 mL, 1×10^8) were added to 4.5 mL of degassed PBS (pH 7.4 ± 0.1) in a glass vial and the contents agitated periodically at 37 °C. As the O_2MBs float at the top of the PBS solution they were in direct contact with air in the headspace of the open vial. The amount of dissolved O_2 in the PBS solution was determined using a dissolved oxygen metre and was measured for 4.5 min before and 14.5 min after ultrasound treatment. As a control, experiments using PFBMBs were also conducted. The results are shown in Fig. 3 and illustrate that the O_2MBs effectively retain their O_2 until destruction by the externally applied ultrasound at which point the dissolved oxygen increases by more than 40% 5 min after irradiation. In contrast, the dissolved oxygen in the PFBMB control experiment increased by about 20% 1 min after exposure to ultrasound and then decreased to only 5% at 5 min after exposure to ultrasound. We believe this initial increase in dissolved O_2 in the control preparation was due to ultrasound-mediated agitation of the fluid in the measurement chamber. Nevertheless, the results suggest that the O_2MBs effectively retain oxygen and exposure to ultrasound results in an increase in dissolved oxygen that is sustained for a relatively prolonged period of time in this system. We believe this time frame of both retention and ultrasound-mediated release would facilitate sufficient time to enable targeting of microbubbles and their gas payload to a specific anatomical site and provide an increase in dissolved oxygen in a tissue microenvironment that would be sufficient to support

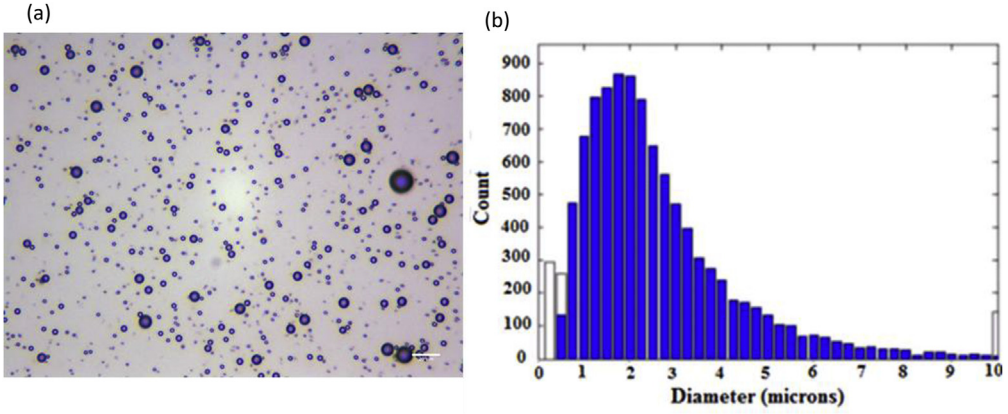

Fig. 1. Photomicrographs taken with a 40× objective lens of the O_2MB after dilution (1:10) in PBS. Scale bar is 20 μm; (b) size distribution of O_2MB after centrifugation obtained from analysis of 30 optical microscope images (the unfilled boxes at the left hand side of the graph represent MB that were detected by the image analysis software but smaller than 450 nm, the optical resolution of the system).

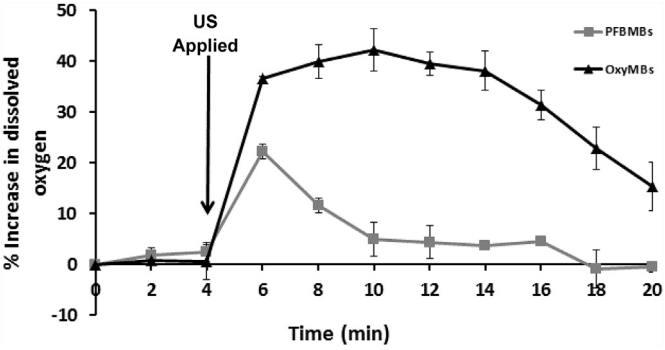

Fig. 3. Plot of % increase in dissolved oxygen for degassed PBS solutions containing either O_2MB or PFBMB. Arrow indicates time of ultrasound application.

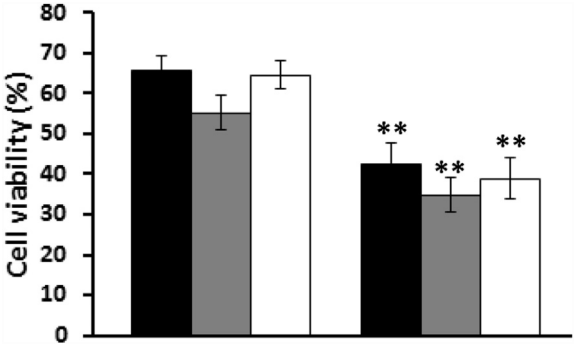

Fig. 5. Plot of cell viability for BxPc-3 (black), MIA PaCa-2 (grey) and PANC-1 (white) cells treated with PFBMB-RB/PFBMB-5FU mix + US (left) or (ii) O_2MB-RB/O_2MB-5FU mix + US (right). Concentrations and US parameters as in Fig. 4. Error bars represent ± the standard error where n = 4 **p < 0.01.

enhanced ROS generation during SDT as suggested by our previously published findings [4].

To enable attachment of the Rose Bengal sensitiser and 5-FU to the avidin functionalised MBs, it was first necessary to biotinylate both compounds. We have already reported the preparation of biotinylated Rose Bengal (**6**) in a previous communication [4]. The rationale for choosing 5-FU instead of gemcitabine was that the synthesis of biotin-5-FU is less challenging and costly than the corresponding biotin-gemcitabine analogue, and would still allow us to evaluate the merit of combining SDT and antimetabolite therapy for the treatment of pancreatic cancer. To prepare biotinylated 5-FU (**5**), biotin-NHS (**1**) was first reacted with aminoethanol to produce the alcohol-functionalised biotin derivative **2** (Scheme 1a). In parallel, 5-FU (**3**) was reacted with chloroacetic acid to produce the corresponding carboxylic acid functionalised 5-FU derivative **4**. Compounds **2** and **4** were then esterified using carbodiimide based chemistry to form biotinylated 5-FU **5**. Both **5** and **6** were mixed separately with avidin functionalised PFBMB and purified by two centrifugation and PBS washing cycles. The conjugates were then mixed together, sparged with O_2 and this O_2MB-RB/O_2MB-5FU mix used directly in the *in vitro* and *in vivo* experiments.

To determine the effectiveness of the combined antimetabolite/SDT treatment *in vitro*, three different pancreatic cancer cell lines that are routinely used in preclinical studies, BxPc-3, MIA PaCa-2 and PANC-1 were seeded into 96 well plates. To simulate the hypoxic environment encountered in a tumour microenvironment, these cells were incubated in an anaerobic cabinet (O_2/CO_2/N_2, 0.1:

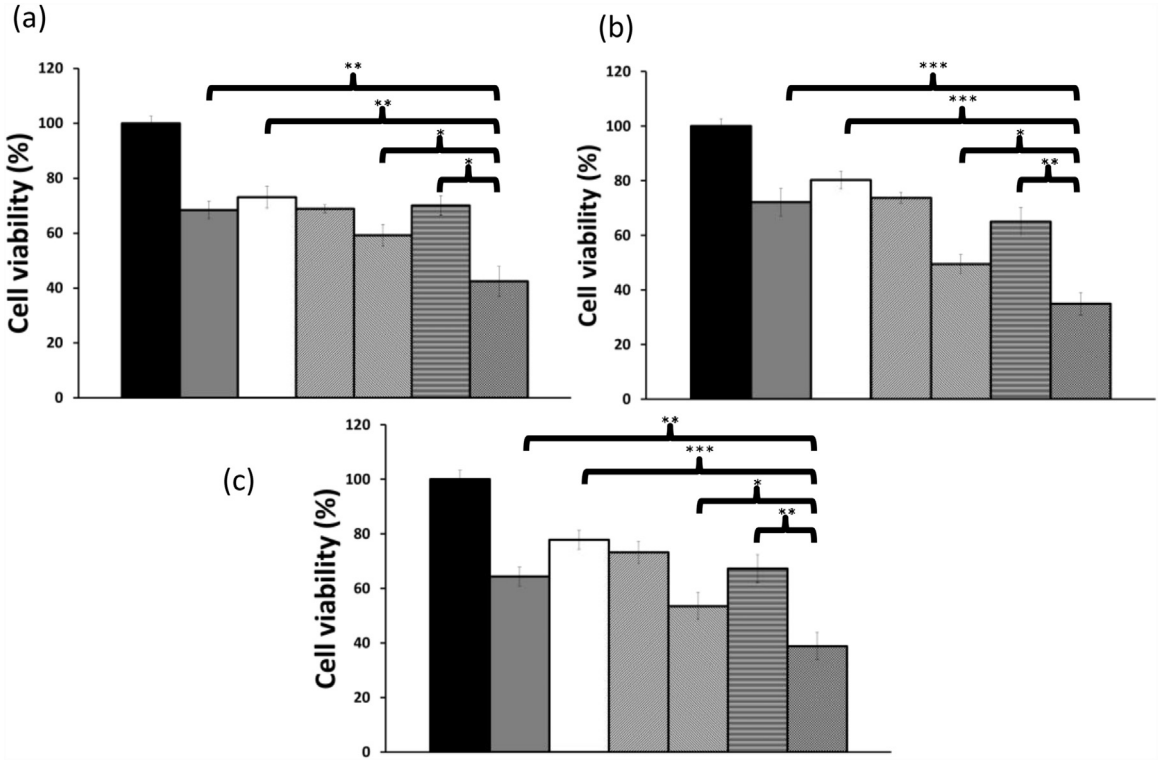

Fig. 4. Plot of cell viability for (a) BxPc-3, (b) MIA PaCa-2 and (c) PANC-1 cells treated with (from left to right) (i) no treatment (ii) gemcitabine (iii) 5-FU (iv) O_2MB-5FU + US (v) O_2MB-RB + US (vi) O_2MB-RB/O_2MB-5FU mix − US and (vii) O_2MB-RB/O_2MB-5FU mix + US. [RB], [5-FU] and [gemcitabine] were kept constant at 5 μM, 100 μM and 100 μM respectively. Ultrasound treatment was delivered for 30 s at frequency of 1 MHz, an ultrasound power density of 3.0 Wcm^{-2} and a duty cycle of 50%, pulse frequency = 100 Hz. Error bars represent ± the standard error where n = 4. *p < 0.05, **p < 0.01 and ***p < 0.001.

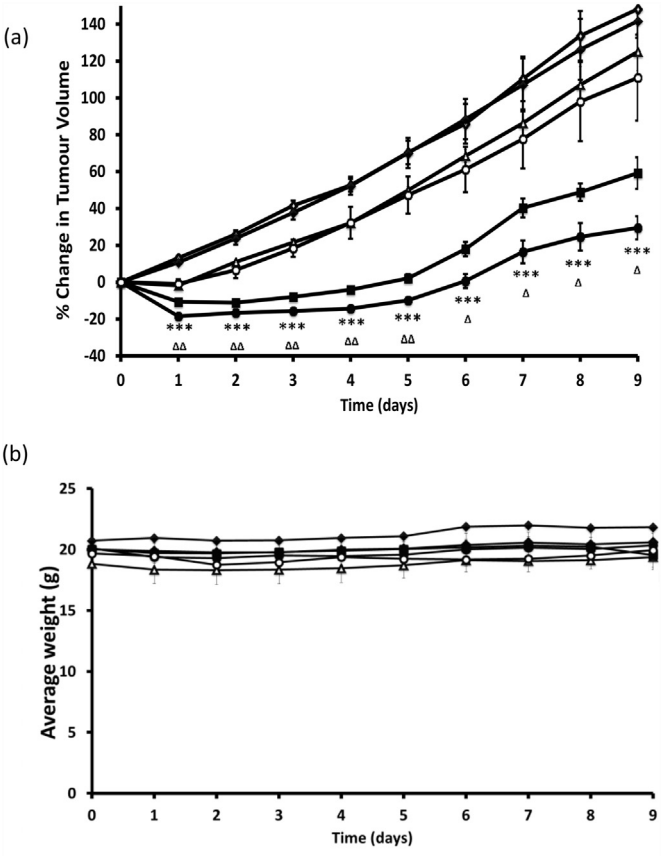

Fig. 6. Plot of (a) % change in tumour volume and (b) average body weight for mice treated with (i) no treatment (open diamonds) (ii) ultrasound only (filled diamonds) (iii) gemcitabine (open triangles) (iv) O_2MB-RB/O_2MB-5FU mix − US (open circles) (v) O_2MB-RB + US (filled squares) (vi) O_2MB-RB/O_2MB-5FU mix + US (filled circles). Not shown for ease of illustration are treatments with 5-FU alone, O_2MB-RB − US, O_2MB-5FU + US, O_2MB-5FU−US. The RB, 5-FU and gemcitabine concentrations were kept constant in each case at 0.184 mg/kg (90.8 μM), 0.115 mg/kg (440 μM) and 0.264 mg/kg (440 μM) respectively. Ultrasound treatment was delivered for 30 s at frequency of 1 MHz, an ultrasound power density of 3.0 Wcm^{-2} and a duty cycle of 50%, pulse frequency = 100 Hz. Error bars represent ± the standard error where n = 4. $^{*}p < 0.05$, $^{**}p < 0.01$ and $^{***}p < 0.001$ for (vi) compared to (i) and $^{\Delta}p < 0.05$, $^{\Delta\Delta}p < 0.01$ and $^{\Delta\Delta\Delta}p < 0.001$ for (vi) compared to (v).

5: 94.9 v/v/v) for 3 h prior to treatment. Cells were then treated with either (i) vehicle only, (ii) gemcitabine, (iii) 5-FU, (iv) O_2MB-5FU + US, (v) O_2MB-RB + US, (vi) O_2MB-RB/O_2MB-5FU mix − US and (vii) O_2MB-RB/O_2MB-5FU mix + US. In all experiments the amount of RB, 5-FU and gemcitabine used was kept constant at 5 μM, 100 μM and 100 μM respectively. Following treatment, the cells remained in the anaerobic cabinet for a further 3 h at which point the treatment solution was removed, fresh media added and the cells incubated in normoxic conditions for a further 21 h. The effect of treatment was then determined using the MTT cell viability assay [16]. The results, shown in Fig. 4, reveal that a statistically significant reduction in viability was observed in all three cell lines for cells treated with the combined SDT/antimetabolite therapy (i.e. O_2MB-RB/O_2MB-5FU mix + US) compared to that of cells treated with either antimetabolite therapy alone (i.e. 5-FU or gemcitabine). Indeed, a statistically significant reduction in viability was also observed for cells treated with the combined therapy relative to that of cells treated with SDT treatment alone (i.e. O_2MB-RB + US). We have previously shown that the SDT effect observed in such hypoxic conditions is greatly enhanced through the use of O_2MBs and this was again confirmed in the current study by comparing the difference in the cytotoxicity between the O_2MB-RB/

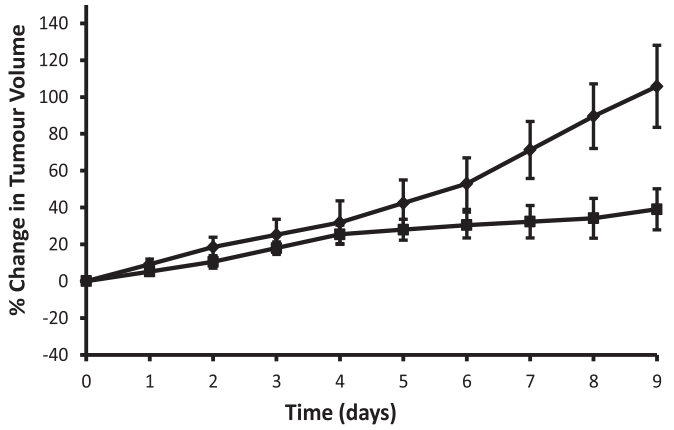

Fig. 7. Plot of % change in tumour volume for mice treated with IP gemcitabine (120 mg/kg on days 0, 3 and 8) (filled squares) or vehicle only (filled diamonds). Error bars represent ± the standard error where n = 4.

O_2MB-5FU mix with ultrasound treatment and an otherwise identical mix of PFBMB conjugates with ultrasound treatment (Fig. 5). Indeed, statistically significant ($p < 0.01$) reductions in cell viability of over 20% were observed for all three cell lines treated with the O_2MB conjugates compared to the PFBMB conjugates. Collectively, the results shown in Figs. 4 and 5 clearly highlight the benefit gained when SDT is combined with antimetabolite therapy, particularly in hypoxic environments where O_2MBs can provide additional O_2 to improve the SDT effect.

Having established the therapeutic benefit of combined SDT/antimetabolite therapy *in vitro*, the next step was to determine if a similar effect would be observed *in vivo*. Ectopic human xenograft BxPC-3 tumours were established in the rear dorsum of SCID mice. We have previously shown these tumours to be extremely hypoxic with a ppO_2 of 2 mmHg (<1%) [4]. Once the tumours had reached an average size of 218 mm^3, the mice were separated into ten groups (n = 4 in each group). Groups 1 and 2 received the O_2MB-RB/O_2MB-5FU mix ± US; groups 3 and 4 the O_2MB-RB ± US; groups 5 and 6 the O_2MB-5FU ± US; group 7 gemcitabine treatment alone, group 8 5-FU treatment alone, group 9 ultrasound treatment only and group 10 was untreated. Where applicable, the amount of RB and 5-FU was kept constant at 0.184 mg/kg (90.8 μM) and 0.115 mg/kg (440 μM) respectively, while the gemcitabine concentration used was 0.264 mg/kg (440 μM). After treatment, the tumour volume was measured daily for 9 days and the % change in tumour volume for each group plotted as a function of time. For ease of interpretation, only results from six of the ten groups are shown in Fig. 6a with the remainder shown in Fig. S4. These results reveal a dramatic reduction in tumour volume for mice treated with the combined SDT/antimetabolite therapy compared to either gemcitabine or 5-FU treatment alone. Indeed, 9 days after treatment, tumours in mice treated with gemcitabine or 5-FU alone grew by 125.1 and 123.3% respectively, while tumours treated with the O_2MB-RB/O_2MB-5FU mix + US grew by only 29.1% over their original starting volume within the same time period. In addition, there was also a statistically significant reduction in tumour volume for tumours treated with the combined SDT/5-FU therapy (i.e. O_2MB-RB/O_2MB-5FU mix + US) relative to SDT treatment alone (i.e. O_2MB-RB + US) with tumours being on average 30.2% smaller 9 days after treatment. Analysis of the average body weight (Fig. 6b) for animals in each of the groups showed no noticeable reductions over the course of the experiment suggesting the treatments did not produce any acute adverse effects.

In the above in *vivo* experiments, gemcitabine was administered as an intra-tumoral injection at a concentration of 0.264 mg/kg in

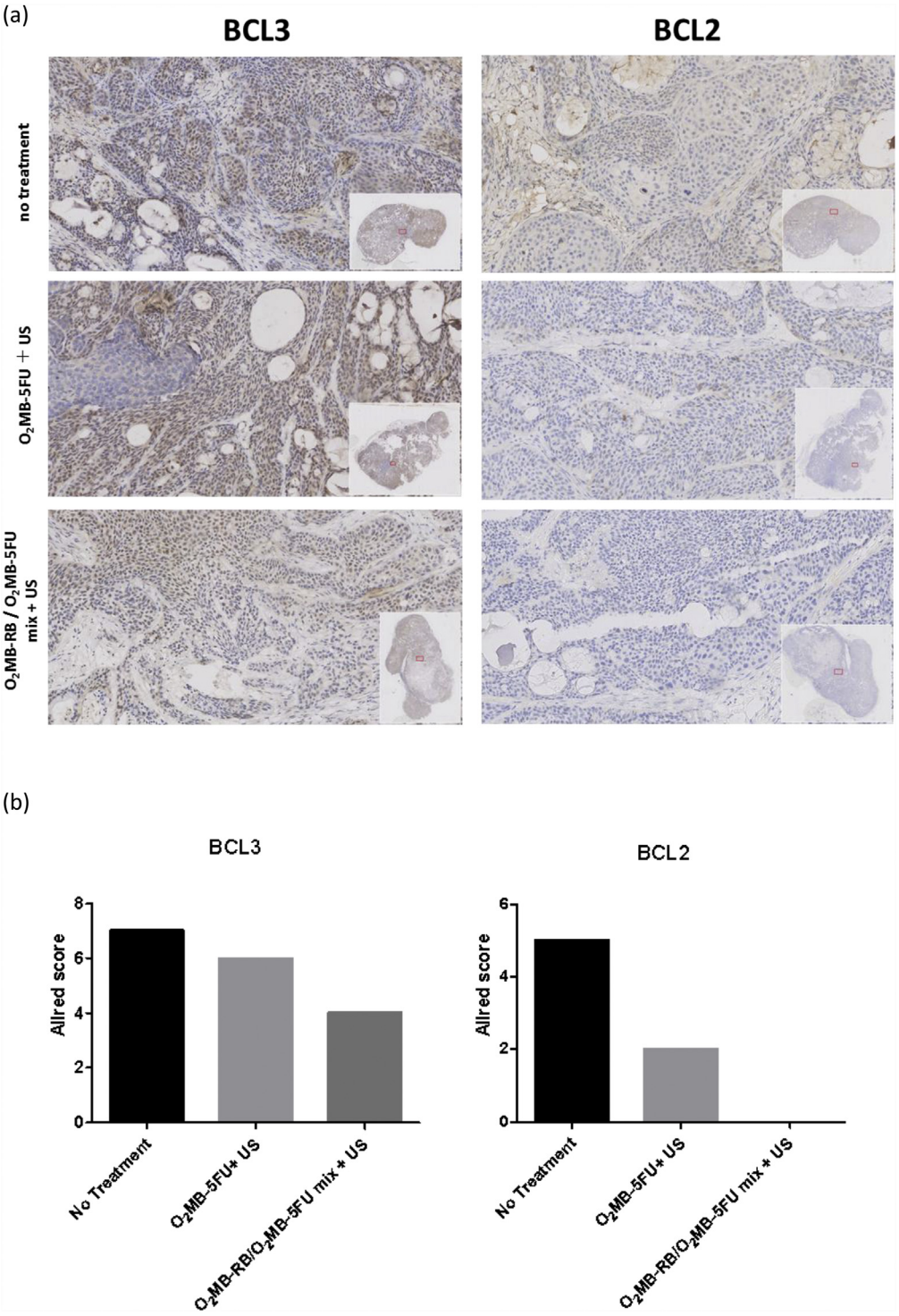

Fig. 8. (a) Bcl3 and Bcl2 protein expression using immunohistochemistry. The inner image is the whole section and the main image is a selected area with ×20 magnification. (b) Histology scoring for Bcl3 and Bcl2 expression.

order to provide a direct molar comparison with the amount of 5-FU used (440 μM). Even though this amount was delivered directly to the tumour it is significantly less than the normal systemic dose of gemcitabine (120 mg/kg) used in mice [21]. In order to compare the effectiveness of the combined SDT/5-FU therapy against systemic gemcitabine therapy, we treated mice bearing ectopic BxPC-3 tumours with gemcitabine (120 mg/kg) administered by intraperitoneal (IP) injection on days 0, 3 and 8. Tumour volume was measured daily as before and compared to untreated animal controls. These results (Fig. 7) demonstrate that while the tumour volume in the control group increased by about 100%, tumour volume increased by 38% in the gemcitabine treated group and at no point in the therapy did the tumour volume decrease below the starting tumour volume. In contrast, with a single treatment, for the combined SDT/5FU therapy (Fig. 6) the tumour volume decreased below the initial treatment volume and remained so up

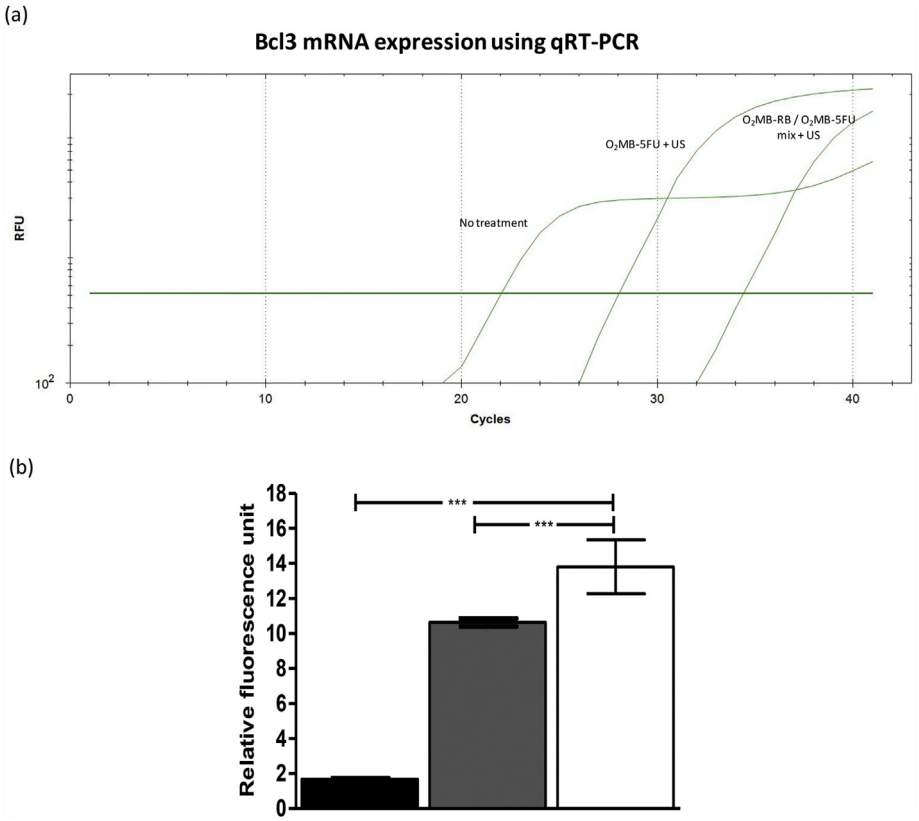

Fig. 9. (a) Quantitative RT-PCR mRNA expression of Bcl3. (b) Plot of Bcl3 gene expression profiles for (i) no treatment (black), (ii) O_2MB-5FU + US (grey) and (iii) O_2MB-RB/O_2MB-5FU mix + US (white). Error bars represent ± the standard deviation where n = 3. ***$p < 0.001$.

to 6 days post treatment while tumours in the gemcitabine group exhibited a 20% increase in tumour volume at day 6. That such dramatic response can be achieved using relatively low amounts of sensitiser/5-FU and following a single treatment is extremely promising and suggests the targeted delivery of such agents could provide enhanced therapeutic benefit with reduced side effects.

We were also interested in probing the effects of combined SDT/5-FU treatment at the molecular level when compared to 5-FU treatment alone. In order to do this, tumours in the control group (i.e. no treatment), the O_2MB-5FU + US group (i.e. 5-FU), and O_2MB-RB/O_2MB-5FU mix + US group (i.e. combined treatment) were harvested at the end of the monitoring period and subjected to immunohistochemistry and qRT-PCR analysis. The immunohistochemistry results revealed that at the protein level, there was Bcl3 and Bcl2 deregulation between both treatment groups and the control group. At this level of analysis, Bcl3 intensity and proportion were higher in the control and 5FU groups but decreased in the combined treatment group. Similarly, Bcl2 protein expression was highest in the control group, decreased in the 5FU group and was undetectable in the combined treatment group (Fig. 8). At the mRNA level, a similar pattern was observed for Bcl3 (Fig. 9a and b) with the ΔΔCt showing significant decreases of approximately 5- and 7-fold for the 5FU and combined treatment groups respectively relative to the control group ($p < 0.001$). Bcl3 is a key member of the NF-κB pathway and is involved in regulating many cellular pathways including survival, proliferation, inflammation and immune response. Bcl3 expression and activation has been associated with increased cellular proliferation or survival, dependent on the tissue and the type of stimuli. Its transcriptional repressor function has been shown to be involved in regulating immune responses as well as the development and activation of immune cells [22]. The fact that Bcl3 expression was deregulated suggests an alteration in the immune response as well as survival and proliferation cell signalling. This was confirmed by the fact that Bcl2, which is an important anti-apoptotic gene [23], was higher in the control but its expression decreased remarkably after the combined treatment. Indeed Bcl2 expression is known to be up-regulated in the majority of primary pancreatic tumours [24] and it has been demonstrated that using Bcl2-spectific siRNA to down-regulate its expression has anti-proliferative and pro-apoptotic effects on pancreatic tumour growth *in vitro* and *in vivo* [25]. More recently, it has been shown that a G-quadruplex-binding compound (MM41) that exhibits anti-tumour activity using the MIA PaCa-2 pancreatic cancer xenograft model, reduced Bcl2 levels by 40% following analysis at the protein level [26]. Taken together, these results indicate a marked effect on cellular signalling pathways as a result of the combined SDT/5-FU treatment and suggest that SDT could provide significant therapeutic benefit for pancreatic cancer patients when employed together with conventional chemotherapy-based regimes. Understanding the underlying molecular mechanisms involved in signalling pathway alteration and control may lead to better optimisation of SDT and enhance its effectiveness in the treatment and prevention of this aggressive form of cancer.

If our O_2MB platform is to be suitable for clinical translation, the MB suspension will need to be administered intravenously and the MBs disrupted at the tumour site using appropriate ultrasound conditions. Such a strategy should enhance localisation of the sensitiser/chemotherapeutic and increase tumour pO_2 at the tumour site. To test the feasibility of such an approach we prepared a biotin functionalised near infrared absorbing cyanine dye (9) as a surrogate for RB and 5-FU (Scheme 2). The UV–Vis and fluorescence spectra of 9 (Fig. S6) reveal absorbance (750 nm) and

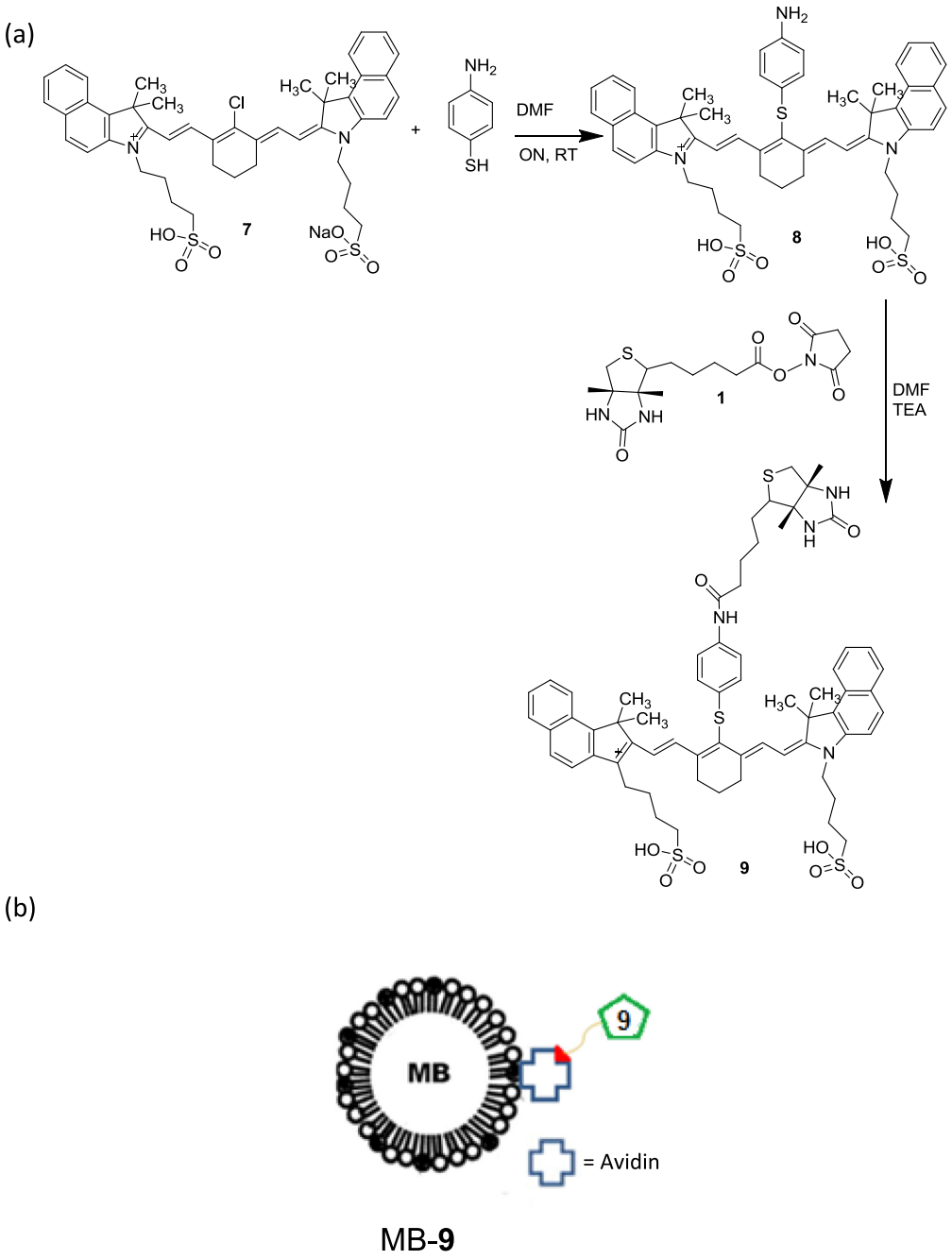

Scheme 2. (a) Synthesis of biotin functionalised NIR absorbing dye (**9**). (b) Schematic representation of the MB-**9** conjugate using in the imaging experiments.

emission maxima (818 nm) in the NIR region making this compound ideal for *in vivo* imaging. 9 was loaded onto the MB surface following the same procedure used for RB and 5-FU. The O_2MB-9 conjugate was then administered intravenously via the tail vein of athymic nude mice bearing ectopic Bx-PC3 tumours. Ultrasound was applied directly to the tumour during and for 3 min after IV administration. Control experiments in the absence of ultrasound were used for comparative purposes. The mice were imaged before, 5 and 30 min after administration using an IVIS whole body imaging system. Representative images (Fig. 10a) reveal strong tumour fluorescence 30 min after treatment for mice in the ultrasound treated group while mice in the control group showed negligible tumour fluorescence, with most of the emission observed from the liver region. When the intensity of tumour fluorescence was measured relative to the pre-treatment value (Fig. 10b), a statistically significant 7-fold enhancement was observed for the ultrasound treated group relative to the control group, 30 min following treatment ($p < 0.01$). Furthermore, when either O_2MB or PFBMB were administered to tumour-bearing animals by tail vein injection and subsequently treated with ultrasound, protein extracts from surgically-excised tumours revealed a significant decrease in Hif-1α in tumours treated with the O_2MB (Fig. 10c). These results suggest that the application of ultrasound to the tumour, during and immediately after administration of the O_2MB-9 conjugate, facilitates stimulus-dependant destruction of the MBs in the tumour vasculature which in turn facilitates release

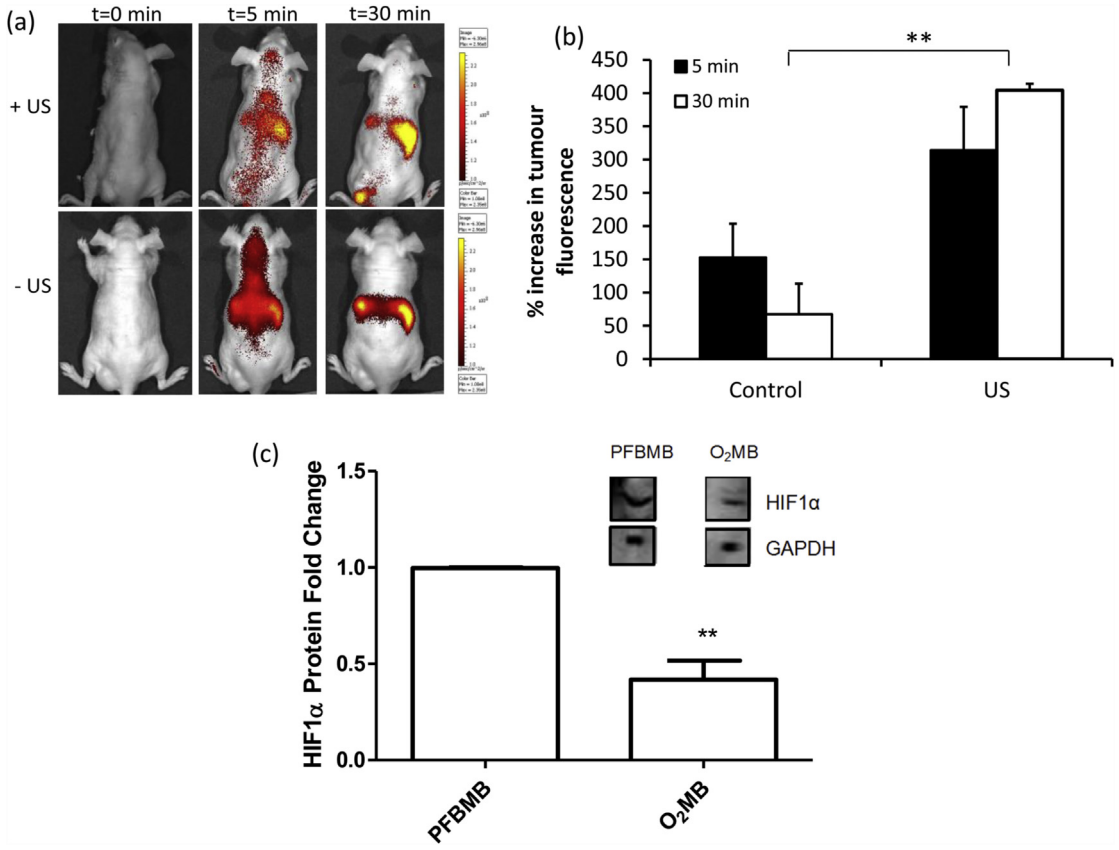

Fig. 10. (a) Representative fluorescence images of nude mice bearing ectopic BxPC-3 tumours before (t = 0), 5 min after (t = 5) and 30 min after (t = 30) intravenous administration of the MB-**9** conjugate with (+US) or without (−US) ultrasound applied to the tumour during IV injection. (b) Plot of % increase in tumour fluorescence recorded 5 and 30 min after intravenous administration of MB-**9** conjugates with (US) or without (control) ultrasound applied to the tumour during IV injection. Increase in intensity measured relative to tumours before treatment. Error bars represent ± SEM where n = 3. (c) Densitometry data (compared to loading control GAPDH) showing tumour Hif1α protein expression for mice treated with an IV suspension of O_2MB or PFBMB. Inset shows a representative Western Blot image of HIF1α protein expression in tumours treated with an IV suspension of O_2MB or PFBMB. Error bars represent ±SEM where n = 3. *p < 0.05, **p < 0.01 and ***p < 0.001.

of both O_2 and the attached payload in a targeted manner. The end result is an increase in tumour pO_2 as evidenced by reduced expression of Hif1α protein and a greater concentration of drug in the tumour as evidenced by the enhanced fluorescence of 9.

4. Conclusions

In summary, we have prepared biotin-RB and 5-FU derivatives suitable for attachment to the surface of a platform consisting of avidin-functionalised MBs filled with O_2 gas. The MBs have been shown to retain their O_2 until they are disrupted using externally applied ultrasound. We have also demonstrated that combining sonodynamic and antimetabolite therapy using the O_2MB conjugates provided enhanced cytotoxicity in three different pancreatic cancer cell lines cultured under anaerobic conditions when compared with cytotoxicity yielded by either treatment alone. Similarly, treatment of ectopic BxPC-3 tumours with the combined therapy led to a statistically significant reduction in tumour volume when compared with the efficacy of either therapy alone. These results suggest that combined sonodynamic and antimetabolite therapy using ultrasound-responsive O_2MBs could provide a promising alternative to chemotherapy for the treatment of locally advanced pancreatic cancer and could also be effective as a neo-adjuvant therapy. Furthermore, we have shown that our avidin-functionalised MB platform is an effective vehicle for the targeted delivery of biotinylated payloads to ectopic BxPC-3 tumours upon application of externally applied ultrasound. In addition, this is the first study characterising the effect of SDT at the molecular genetic level and our results have shown that this treatment approach has an effect on the expression of immune-associated signalling pathways. Future work in our laboratory seeks to develop this technology to enable IV delivery and targeted destruction of the O_2MB conjugates in an orthotropic pancreatic tumour model. We will also focus on further characterizing the effect of SDT on cellular signalling pathways, with a view toward understanding the underlying mechanisms that mediate this therapy. We believe that optimised dosing and multiple treatments can further improve on the results reported in this manuscript and offer pancreatic cancer patients the prospect of a targeted treatment that minimises adverse effects but at the same time provides an enhanced local therapy with an improved outcome.

Acknowledgements

JFC thanks Norbrook Laboratories Ltd. for funding an endowed chair. CMcE acknowledges the Department of Employment and Learning (DEL) for a PhD studentship. ES and JO thank the Engineering and Physical Sciences Research Council for support through grant EP/I021795/1.

Appendix A. Supplementary data

Supplementary data related to this article can be found at http://dx.doi.org/10.1016/j.biomaterials.2015.11.033.

References

[1] J. Li, M.G. Wientjes, J.L. Au, Pancreatic cancer: pathobiology, treatment options, and drug delivery, AAPS J. 12 (2010) 223–232.

[2] S.A. Badger, J.L. Brant, C. Jones, J. McClements, M.B. Loughrey, M.A. Taylor, T. Diamond, L.D. McKie, The role of surgery for pancreatic cancer: a 12-year review of patient outcome, Ulst. Med. J. 79 (2010) 70–75.

[3] A. Stathis, M.J. Moore, Advanced pancreatic carcinoma: current treatment and future challenges, Nat. Rev. Clin. Oncol. 7 (3) (2010) 163–172.

[4] C. McEwan, J. Owen, E. Stride, C. Fowley, H. Nesbitt, D. Cochrane, C.C. Coussios, M. Borden, N. Nomikou, A.P. McHale, J.F. Callan, Oxygen carrying microbubbles for enhanced sonodynamic therapy of hypoxic tumours, J. Control Release 203 (2015) 51–56.

[5] (a) K. Plaetzer, M. Berneburg, T. Kiesslich, T. Maisch, New applications of photodynamic therapy in biomedicine and biotechnology, BioMed Res. Int 2013 (2013) 161362;
(b) W. Hiraoka, H. Honda, L.B. Feril Jr., N. Kudo, T. Kondo, Comparison between sonodynamic effect and photodynamic effect with photo sensitizers on free radical formation and cell killing, Ultrason. Sonochem 13 (6) (2006) 535–542;
(c) I. Rosenthal, J.Z. Sostaric, P. Riesz, Sonodynamic therapy – a review of the synergistic effects of drugs and ultrasound, Ultrason. Sonochem. 11 (6) (2004) 349–363.

[6] D. Costley, C. Mc Ewan, C. Fowley, A.P. McHale, J. Atchison, N. Nomikou, J.F. Callan, Treating cancer with sonodynamic therapy: a review, Int. J. Hyperth. 31 (2015) 107–117.

[7] J.R. Starkey, A.K. Rebane, M.A. Drobizhev, Gong A. Meng, A. Elliot, et al., New two-photon activated photodynamic therapy sensitizers induce xenograft tumor regressions after near-IR laser treatment through the body of the host mouse, Clin. Cancer Res. 14 (2008) 6564–6573.

[8] N. Nomikou, C. Fowley, N.M. Byrne, B. McCaughan, A.P. McHale, J.F. Callan, Microbubble-sonosensitiser conjugates as therapeutics in sonodynamic therapy, Chem. Commun. 48 (2012) 8332–8334.

[9] M.E. Burkard, H.D. Vanliew, Oxygen-transport to tissue by persistent bubbles - theory and simulations, J. Appl. Physiol. 77 (6) (1994 Dec) 2874–2878.

[10] A. Yuen, D. Begona, The impact of hypoxia in pancreatic cancer invasion and metastasis, Hypoxia 2 (2014) 91–106.

[11] M.G. Lee, S.H. Lee, S.J. Lee, Y.S. Lee, J.H. Hwang, J.K. Ryu, Y.T. Kim, D.U. Kim, S.M. Woo, 5-Fluorouracil/leucovorin combined with irinotecan and oxaliplatin (FOLFIRINOX) as second-line chemotherapy in patients with advanced pancreatic cancer who have progressed on gemcitabine-based therapy, Chemotherapy 59 (2013) 273–279.

[12] D.B. Longley, D.P. Harkin, P.G. Johnston, 5-fluorouracil: mechanisms of action and clinical strategies, Nat. Rev. Cancer 3 (2003) 330–338.

[13] K. Tomankova, H. Kolarova, P. Kolar, K. Kejlova, D. Jirova, Study of cytotoxic effect of photodynamically and sonodynamically activated sensitizers in vitro, Toxicol Vitro 23 (8) (2009) 1465–1471.

[14] S. Kang, L. Mou, W.J. Brouillette, P.E. Prevelige Jr., Rapid Commun. Mass Spectrom. 23 (11) (2009) 1719–1726.

[15] N.S. James, Y. Chen, P. Joshi, T.Y. Ohulchanskyy, M. Ethirajan, M. Henary, L. Strekowsk, R.K. Pandey, Evaluation of polymethine dyes as potential probes for near infrared fluorescence imaging of tumors: part – 1, Theranostics 3 (9) (2013) 692–702.

[16] A.P. McHale, L. McHale, Use of a tetrazolium based colorimetric assay in assessing photoradiation therapy in vitro, Cancer Lett. 41 (1988) 315–321.

[17] D.C. Allred, J.M. Harvey, M. Berardo, G.M. Clark, Prognostic and predictive factors in breast cancer by immunohistochemical analysis, Mod. Pathol. 11 (2) (1998) 155–168.

[18] (a) R.A. Hamoudi, A. Appert, H. Ye, A. Ruskone-Fourmestraux, B. Streubel, A. Chott, M. Raderer, L. Gong, I. Wlodarska, C. Wolf-Peeters, K.A. Maclennan, L. deLeval, P.G. Isaacson, M.Q. Du, Differential expression of NF-kappaB target genes in MALT lymphoma with and without chromosome translocation: insights into molecular mechanism, Leukemia 24 (8) (2010) 1487–1497;
(b) Y. Bi, N. Zeng, E. Chanudet, Y. Huang, R.A. Hamoudi, H. Liu, G. Dong, A.J. Watkins, S.C. Ley, L. Zou, R. Chen, X. Zhu, M.Q. Du, A20 inactivation in ocularadnexal MALT lymphoma, Haematologica 97 (2012) 926–930.

[19] (a) M.A. Borden, M.L. Longo, Oxygen permeability of fully condensed lipid monolayers, J. Phys. Chem. B 108 (2004) 6009–6016;
(b) P.A. Mountford, S.R. Sirsi, M.A. Borden, Condensation phase diagrams for lipid-coated perfluorobutane microbubbles, Langmuir 30 (2014) 6209–6218;
(c) S. Garg, A.A. Thomas, M.A. Borden, The effect of lipid monolayer in-plane rigidity on in vivo microbubble circulation persistence, Biomaterials 34 (2013) 6862–6870;
(d) J.J. Kwan, M. Kaya, M.A. Borden, P.A. Dayton, Theranostic oxygen delivery using ultrasound and microbubbles, Theranostics 2 (12) (2012) 1174.

[20] W.K. Mitchell, B.E. Phillips, J.P. Williams, D. Rankin, K. Smith, J.N. Lund, P.J. Atherton, Development of a new Sonovue™ contrast–enhanced ultrasound approach reveals temporal and age–related features of muscle microvascular responses to feeding, Physiol. Rep. 1 (5) (2013) e00119.

[21] N.R. Michaud, Y. Wang, K.A. McEachern, J.J. Jordan, A.M. Mazzola, A. Hernandez, S. Jalla, J.W. Chesebrough, M.J. Hynes, M.A. Belmonte, L. Wang, J.S. Kang, J. Jovanovic, N. Laing, D.W. Jenkins, E. Hurt, M. Liang, C. Frantz, R.E. Hollingsworth, D.M. Simeone, D.C. Blakey, V. Bedian, Novel neutralizing hedgehog antibody MEDI-5304 exhibits antitumor activity by inhibiting paracrine hedgehog signaling, Mol. Cancer Ther. 13 (2) (2014) 386–398.

[22] (a) J. Wessells, M. Baer, H.A. Young, E. Claudio, K. Brown, U. Siebenlist, et al., BCL-3 and NF-kappaB p50 attenuate lipopolysaccharide-induced inflammatory responses in macrophages, J. Biol. Chem. 279 (2004) 49995–50003;
(b) H. Kuwata, Y. Watanabe, H. Miyoshi, M. Yamamoto, T. Kaisho, K. Takeda, et al., IL-10-inducible Bcl-3 negatively regulates LPS-induced TNF-alpha production in macrophages, Blood 102 (2003) 4123–4129.

[23] D.L. Vaux, S. Cory, J.M. Adams, Bcl-2 gene promotes haemopoietic cell survival and cooperates with c-myc to immortalize pre-B cells, Nature 335 (6189) (1988) 440–442.

[24] D. Campani, I. Esposito, U. Boggi, D. Cecchetti, M. Menicagli, F. De Negri, L. Colizzi, M. Del Chiaro, F. Mosca, G. Fornaciari, G. Bevilacqua, J. Pathol. 194 (4) (2001) 444–450.

[25] M. Ocker, D. Neureiter, M. Lueders, S. Zopf, M. Ganslmayer, E.G. Hahn, C. Herold, D. Schuppan, Gut 54 (9) (2005) 1298–1308.

[26] S.A. Ohnmacht, C. Marchetti, M. Gunaratnam, R.J. Besser, S.M. Haider, G. Di Vita, H.L. Lowe, M. Mellinas-Gomez, S. Diocou, M. Robson, J. Sponer, B. Islam, R.B. Pedley, J.A. Hartley, S. Neidle, Sci. Rep. 16 (5) (2015) 11385, http://dx.doi.org/10.1038/srep11385.